ADVANCED FUNCTIONAL MATERIALS
www.afm-journal.de

Quantitative and Real-Time Evaluation of Pressure on Brain Spatula with Wireless and Compact Sensing System

*Yongqing Wang, Chengjun Zhang, Xianglin Meng, Qisheng Zhang, Haoyu Li, Feng Chen, Qing Yang, Weiqiang Zhang, Yuanjin Zheng, and Sicheng Chen**

The brain spatula has been an essential neurosurgical instrument since the early 20th century, when medical advancements enabled surgeons to operate deep intracranially for the first time. Monitoring the brain retraction pressure, especially at an early stage of the intradural procedure, is useful in preventing brain damage or postoperative cerebral swelling. Unfortunately, there is still a lack of effective methods that meet the demand for quantitative and real-time evaluation of applied pressure on brain tissue. In this study, a compact and wireless sensing system, encapsulated by soft biocompatible materials, for quantitatively assessing the pressure between brain tissue and a spatula, is proposed. The absence of physical tethers and the ion gel-based construction of the micro-structured sensor represent key defining features, resulting in high measurement accuracy of 1.0/N with reliable water-proof capabilities. Moreover, these sensors can be linked to a server network or mobile client for possible brain damage alerts as important safety addition. With our devices, detailed pressure data on retracting operations can be collected, analyzed, and stored for medical assistance as well as to improve surgery quality.

1. Introduction

Deep-seated brain lesions can be difficult to access without causing significant trauma to the overlying cortex. In the early period, Cusing and Horsley introduced the first brain spatula that presented a handheld metallic ribbon, for retracting, mobilizing, and manipulating the delicate brain parenchyma to gain an optimal view of the surgical field (**Figure 1**a).[1–3] Brain injuries associated with improper retractions can be caused by the focal spatula pressure, depending on the difficulty of the procedure, the skill of the operating team, and the criteria used to define brain injury (parenchymal hematomas, aphasia, hemiparesis, and numbness).[4–6] A considerable reduction in regional cerebral blood flow has been demonstrated with brain retraction at a pressure of ≈25 mm Hg.[7–9] Therefore, continuous measurement of this pressure value with smart devices is a powerful route for safer surgical procedures but has not yet been fully exploited.

Some innovations have been introduced with the new development on the brain retractor system and cerebral protection, including assembling the strain gauges or paired electrodes for pressure sensing.[10,11] The shape deformation of the spatula can be revealed by the resistive change or on-off conditions. Unfortunately, these devices are far from compact, sensitive and precise enough, and do not meet the need for efficient signal collection in complex environments without restricting the surgeon's freedom.[12] Besides, the accuracy of such indirect measurement of spatula pressure is closely correlated with the holding fulcrum position and limited by the wire transmission. Direct detection of precise pressure can be realized by various small flexible sensors, including capacitive, triboelectrical, and resistive types,[13–18] which are potential candidates for the spatula components. Capacitive and triboelectrical pressure sensors usually possess extremely high sensitivities,[19,20] while they can also sensitive to the surrounding dielectric environment (blood flow). In contrast, resistive sensors are more capable of this changeable environments. Despite the availability of several wireless readout wearable devices,[21–23] it is still hard to maintain reliable data acquisition quality on a spatula owing to the limited area between electronic components.

Here, we report a strategy that exploits a wirelessly communicating, compact and low-profile sensing system upon

Y. Wang, Q. Zhang
School of Geophysics and Information Technology
China University of Geosciences
Beijing 100083, China
Y. Wang, Y. Zheng, S. Chen
School of Electrical and Electronic Engineering Nanyang Technological University
50 Nanyang Avenue, Singapore 639798, Singapore
E-mail: sicheng.chen@ntu.edu.sg
C. Zhang, Q. Yang
School of Mechanical Engineering
Xi'an Jiaotong University
Xi'an 710049, China
X. Meng
Department of Critical Care Medicine
The First Affiliated Hospital of Harbin Medical University
Harbin 150001, China
H. Li, F. Chen
School of Electronics & Information Engineering
Xi'an Jiaotong University
Xi'an 710049, China
W. Zhang
School of Aerospace Science and Technology
Xidian University
Xi'an 710049, China

The ORCID identification number(s) for the author(s) of this article can be found under https://doi.org/10.1002/adfm.202210596.

DOI: 10.1002/adfm.202210596

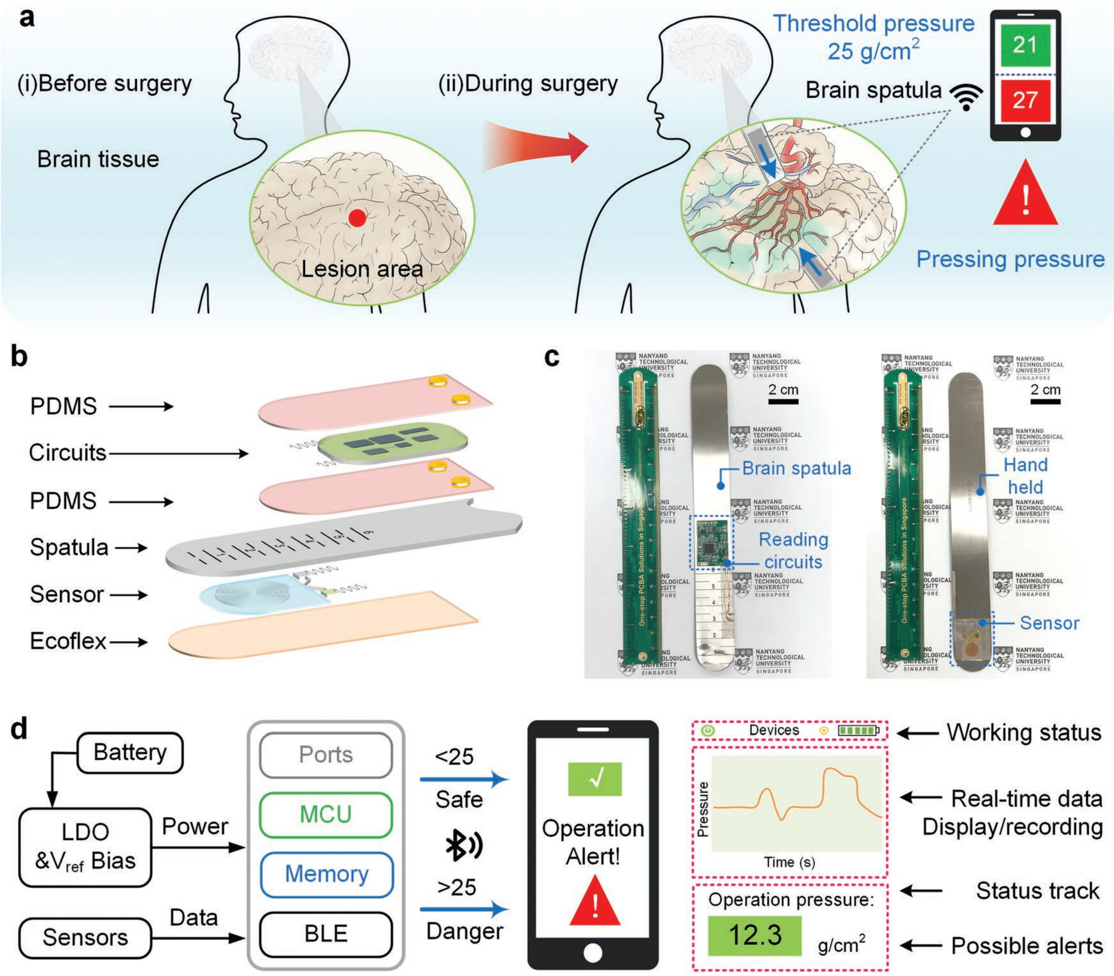

Figure 1. Main idea of the designed wireless sensing system upon brain spatula. a) Schematic view of the brain spatula for subtle surgery. b) Exploded schematic illustration of the active subsystems, enclosure architectures, and customized sensors. c) Images that demonstrate assembling components with initial encapsulations. d) Block diagram of the system operation with user interface (Note S3, Supporting Information).

brain spatula, capable of collecting real-time applied pressure on brain tissue at high data quality in a non-invasive way. This device softly couples to a stainless spatula to capture signals with stable performance under blood environment, providing a more comprehensive perspective on brain tissue surgery. The high-sensitivity ion gel-based resistive film is applied for repeatable and low-pressure sensing. Micro-structures with a pillar width of <200 µm on the resistive layer are obtained using femtosecond laser for rapid and mass production of sensor patterns to reduce personal training and process optimization. Using paired involute electrodes instead of neighboring top and down electrode plates with their substrates, conformal, and compact sensors are fabricated for more convenient application on brain spatula. Smart peripheral integrated reading circuits also ensure the real-time data transmission from held brain spatula to monitoring mobile clients for medical assistance and direct visual observation. Unique Advantages for the proposed wireless and compact sensing system are summarized in Note S1 (Supporting Information). Besides, the summary of sensitivity and pressure testing range of flexible pressure sensors is given in Table S1 (Supporting Information).

2. Results and Discussion

2.1. Engineering Mechanics of the Device

The Brain Spatula offers a broad range of benefits for neurosurgeons. Its intended use is to maintain two portions of brain parenchyma away from each other, with the purpose of revealing hidden cerebral structures, to gain an optimal view of the lesion area (Figure 1a). Most of the standard brain spatula is made of stainless steel with a total length of approximately 20 cm. To quantitatively evaluate the applied pressure between brain tissue and spatula, direct sensing and recording of the operation data provide more intuitive information and timely operation guidance. The safe applied pressure lies between 20 to 30 mm Hg for most occasions; thus we assume a certain threshold of 25 g cm^{-2} (19 mm Hg) here. Figure 1b outlines the overall device layout, with images that demonstrate assembling components with initial encapsulations in Figure 1c. The design incorporates a small customized sensor (resistive and flexible pixel), waterproof encapsulation, peripheral electronic components, and biocompatible adhesive sheets (Note S2, Supporting Information). The electronic part consists, more specially, of a thin printed circuit board (PCB) based on an 80 µm thick middle polyimide supporting layer with 18 µm thick patterned copper (Cu) traces on the top and bottom surfaces. Immersion gold is used upon annealed Cu for more reliable solderability in the extra process. The electronic subsystems mainly include i) a customized readout circuit for precise resistance sensing, with strong anti-interference ability, ii) a microcontroller (MCU, nRF 52832) for acquiring data from the reading circuit and communicating the results wirelessly via Bluetooth Low Energy protocols, and iii) a reserved power supply interface for optional rechargeable 150 mAh lithium-ion polymer battery with programmed wireless charging function (Table S2, Supporting Information). As these subsystems highly rely on rigid, planar off-the-shelf components, they should be subtly integrated in a manner that simultaneously offers soft, shape-compatible mechanics as well as effective data collection. The schemes used here exploit advanced versions of design concepts in stretchable electronics,[24,25] adapted for use with the flexible PCB (fPCB) generally. Special interconnects coated by PDMS mechanically and electrically joint the PCB island of 20×40 mm^2 and sensor island of 10×10 mm^2 (see Figure S1, Supporting Information). Small pieces of flexible cured silicone-gel sheets (smooth-on, 50 µm thick, 0.1 MPa Young's modulus) are used to ensure the insulation features between assembled islands and metal brain spatula.

The pressure sensor rests upon the spatula directly contacting with brain tissue for more accurate detection. Soft silicone gel (Ecoflex, smooth-on) serves as water-proof protection, which is more biocompatible than PDMS material. Encapsulating materials can also be selected from other materials with acceptable softness and biocompatibility, such as hydrogels.[26,27] The PCB island is arranged on the other side in order to make it easier for surgeon to use this spatula. The designed resistive sensor allows a more reliable long communication between the neighboring islands. A reference voltage module is combined with the low-dropout regulator (LDO) for precise resistive measurements (Figure 1d). All the tested data would be processed and presented on a compact user interface for revealing real-time applied pressure parameters and possible operation alerts (Note S3, Supporting Information). These results highlight the customized sensors, subtly integrated circuits, and reasonably designed layouts necessary to accommodate realistic user requirements with stable and reliable sensing ability.

2.2. Design and Characterization of Customized Sensors

Incorporating an elastomer with ionic liquid as the resistive regulator has been explored to be an effective method for pressure sensing.[15,28,29] Deformed ionic materials involve mobile distributed ions, which means deformable ionic sensor devices can sense pressure, strain and even other stimuli. **Figure 2**a describes the fabrication process for the prepared pressure sensor, in which the micro-structured conductive film (blue) and Cu/Ni/Au layers (green and orange) are employed as the resistance and electrodes, respectively. Poly-(vinyl alcohol) (PVA) and phosphoric acid (H_3PO_4) solutions are mixed and cast on a flat glass substrate to be cured, followed by demolding. For the resistive sensing mechanisms, introducing microstructures (e.g., micro-pyramids) can effectively improve the sensing performance, such as sensitivity, limit of detection and response time,[30–32] benefiting from the simultaneous contact area change besides resistive layer conductance. To achieve fine patterns on the cured resistive layer with ultra-high processing resolution, a femtosecond laser (wavelength = 800 nm, repetition frequency = 1 kHz, pulse width = 50 fs) is applied to remove surface materials selectively. Micro-structures with a pillar width of <200 µm can be obtained as seen in Figure 2b. The energy dispersive spectroscopy and scanning electron microscope (SEM) images of the laser-structured ion gel film are also provided in Figures S2 and S3 (Supporting Information). Advantages of the Micro-structures are analyzed in Note S4 (Supporting Information). The size and arrangement of the microstructures can be controlled by adjusting the parameters of the laser processing, such as the laser power and the adjacent distance of the laser scanning,[33] as shown in Figure S4 (Supporting Information). To reduce the sensor thickness for more convenient application on brain spatula, paired involute electrodes are assembled under the resistive layer, instead of neighboring top and down electrode plates with their own polyimide (PI) substrates. The electrodes are required to have low and stable resistance. Thereby, we use layered metal for excellent conductance and high bonding strength with PI materials. The wire gap and width are both 100 µm on flexible PI substrates, with a total thickness of 26 µm (Figure S5, Supporting Information). The Au layer can protect conductive Cu traces from being oxidized and the Ni layer is an ideal transition layer. After assembling the electrodes and resistive layer, encapsulations can be further conducted with PDMS and Ecoflex. The pressure applied on this device can produce re-distributions of functional ion mobilities of H^+ and PO_4^- as well as the deformation of micro-structures upon contacted electrodes, as seen in Figure 2c. The electrical field between electrodes and resistive layer is an essential parameter for output signals. As the flowing current I can be defined to be $nesv$, where n, e, s, and v stand for the electron concentration, electron charge, contact area, and electron migration speed, respectively, the compressed status provides a much larger s between resistive layer and electrode compared with initial device status. The simulated results of unit resistance versus deformed vertical displacement are shown in Figure 2d, where reduced resistance caused by shape-deformation is linearly correlated with displacements. The relationships between displacements and the applied pressure is also demonstrated in the inset figure. Even though the simulated results predict an acceptable linear relationship within the linear elastic range of PVA/H_3PO_4 film, ion mobilities among the film also contributes much to enhance the sensitivities. Therefore, more in suit testing should be examined before final components-assembling on brain spatula.

Converting resistive value to voltage signals can be realized by many reading circuits, including single amplifier circuit and Wheatstone bridge connections.[34,35] The collected voltage signals are processed by a 14-bit analog-to-digital converter (ADC) with high sampling rates, demonstrated in **Figure 3**a. To minimize the required PCB components with smaller occupied area, single amplifier circuit is applied using classic feedback

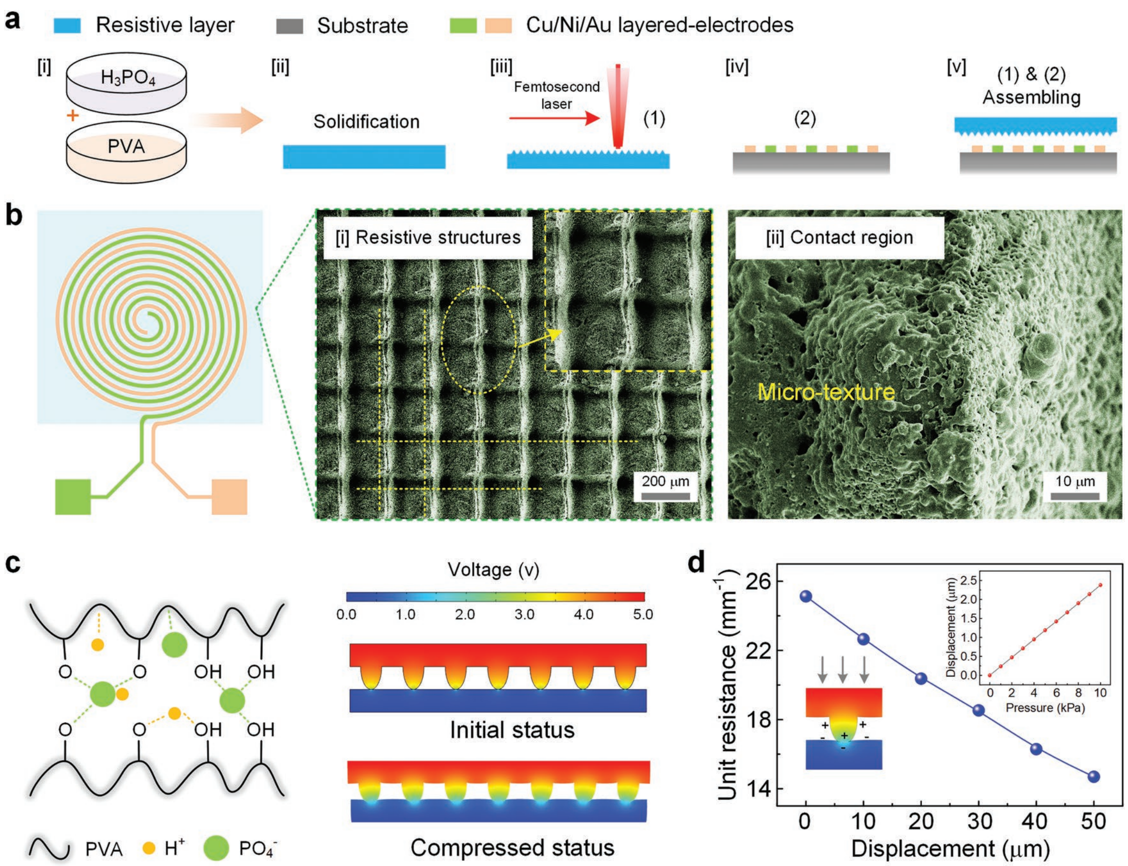

Figure 2. Design and characterization of the customized sensors. a) Fabrication process of the micro-structured ion gel-based resistive sensor and b) corresponding SEM image of surface. c) Simulated results of the resistive performance with increasing pressure. c) Calculated resistance versus vertical displacement under pressure.

connections. The based voltage is 1/11 of the power supply (3.3 V/11 = 0.3 V) and this baseline can be reorganized according to the testing range and reference voltage. The initial resistance and approximate variation resistive range can be evaluated by subtle loading and unloading response (Figure 3b). While the weight of only 5 g (0.005 N) is loaded to the sensor and step-increased, the resistance value response corresponding to the external loading trend, from over 600 to 400 kΩ. A coin of 15 g would lead to a minor resistance of <200 kΩ. Furthermore, the sensor device shows a highly reversible capacitive response during the unloading process under such slight loading applications. This initial assessment of the resistance range is essential for determining the based voltage of applied based voltage (0.3 V) and selecting the proper referenced resistance (50 kΩ). In addition, the pressure test of sensing system at room temperature (27 °C) and 40 °C are provided in Figure S6 (Supporting Information). To comprehensively evaluate the sensing performance, larger loading pressures are detected and summarized as Figure 3c. Each sample point is measured by five times with an error bar demonstrated in the curve. The relative resistance ($\Delta R/R$) presents a sudden decreasing response as long as a slight weight is loaded. A linear relationship with external loading at an effective regime (from 0.1 to 0.5 N) can be obtained, where the threshold of 0.25 N also lies in this regime with easy voltage converting circuits. The equal sensitivity is defined as the slope of the trace, which is calculated to be ≈1.0/N here. The trade-off between sensing range and sensitivity should also be taken into consideration, which means a higher sensitivity represents a narrower detection range for most occasions. These parameters can also be regulated by the fabrication of the devices, for instance, the texture size and the ion concentration. Figure 3d illustrates the sensor exhibits rapid response time of <70 ms, which is comparable to conventional types of flexible pressure sensors, under slight 0.05 N loading conditions. We focused more on the subtle pressure as the sensing device should be suitable for weak force sensing on the brain spatula. We also can see similar repeated response using interval finger touching on the device as shown in Figure 3e. The contact materials are proved to produce limited influence on the sensing stability compared with capacitive and tribo-electrical pressure sensors, where human skin in Figure 3e and metal load in Figure 3d generate same relative resistance under constant loading conditions. Figure 3f presents the excellent repeatability in our long-time monitoring on larger load of 0.3 N (near the threshold value of 0.25 N). we use the sensor to collect pulsed loading over 200 cycles and see that the sensor can maintain stable performance without baseline-shift. These features provide the sensing device with great potential for force detection on brain spatula during surgery.

ADVANCED FUNCTIONAL MATERIALS
www.afm-journal.de

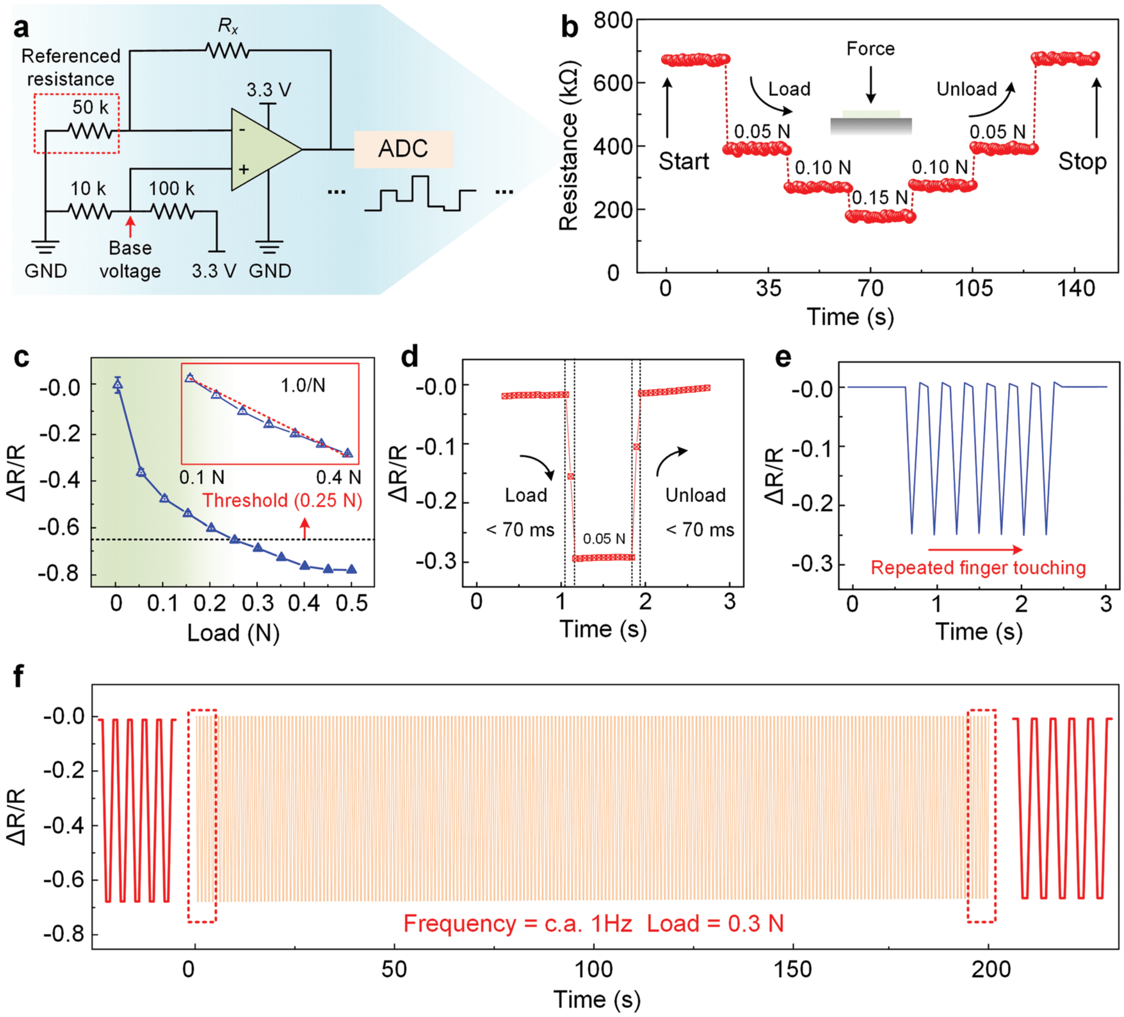

Figure 3. Pressure-sensing performance of the fabricated pressure sensor with a) single amplifier reading circuits. b) Slight step-loading and step-unloading respnse for circuits parameters assessment. c) Relative capacitance ($\Delta R/R$) versus increasing normal load. d) The instant response shows response times of <70 ms. e) Transient response to the finger touching process. f) The excellent repeatability during cycled loading conditions.

2.3. Sensing Performance of Underwater Environments and Applications

With the comprehensive understanding of device sensing features, we further illustrate its utility from dry to underwater conditions to deal with possible blood interference. **Figure 4**a presents the static pressure response of spatula devices resting in normal saline (with 0.9% NaCl). Both the sensors and reading circuits stayed under the liquid level after they had been encapsulated by Ecoflex and PDMS thin films. From the side view of the spatula device, we can see that these encapsulations have negligible influence on its thickness for hand holding. The detected pressure remained constant at 7.2 g cm^{-2} after >3 h. The baseline shift is caused by water pressure and should also be taken into consideration during real-time pressure monitoring. To apply changeable pressure on the spatula under water, we set an obstacle at the bottom of a water tank and press the obstacle using the spatula (Figure 4b). The real-time pressure curve can be displayed on the mobile client for operation alerting if applied pressure reaches over 25.0 g cm^{-2} (Video S1, Supporting Information). Communication stability is an essential factor for efficient data transmission, especially through a wireless protocol. Nrf 52832 has many optional transmitter (Tx) power levels from -20 to 4 dB and -96 dB sensitivity as receiver (Rx). To reduce the power consumption with higher signal transmission capabilities, we set the Tx power to be 0 dB with circuits operation current of 5.3 mA. The received signal strength indicator (RSSI) is always much larger than the receiver sensitivity after the spatula is tested under water.

An obvious benefit for surgery doctors using our spatula devices is to read the immediately applied pressure on brain tissue. However, it is still necessary to build a reliable experience (feel training) for more complex surgery. Figure 4c shows the training process of a volunteer to use the spatula and press on the obstacle. When the experiment started, the volunteer was not clear about the feeling of exact 25.0 g cm^{-2} and the pressure suddenly exceeded the threshold. That is also common for many inexperienced surgeries. After holding the spatula for a few seconds to remember this feeling and removing it, the volunteer attempted to touch the obstacle again. The following

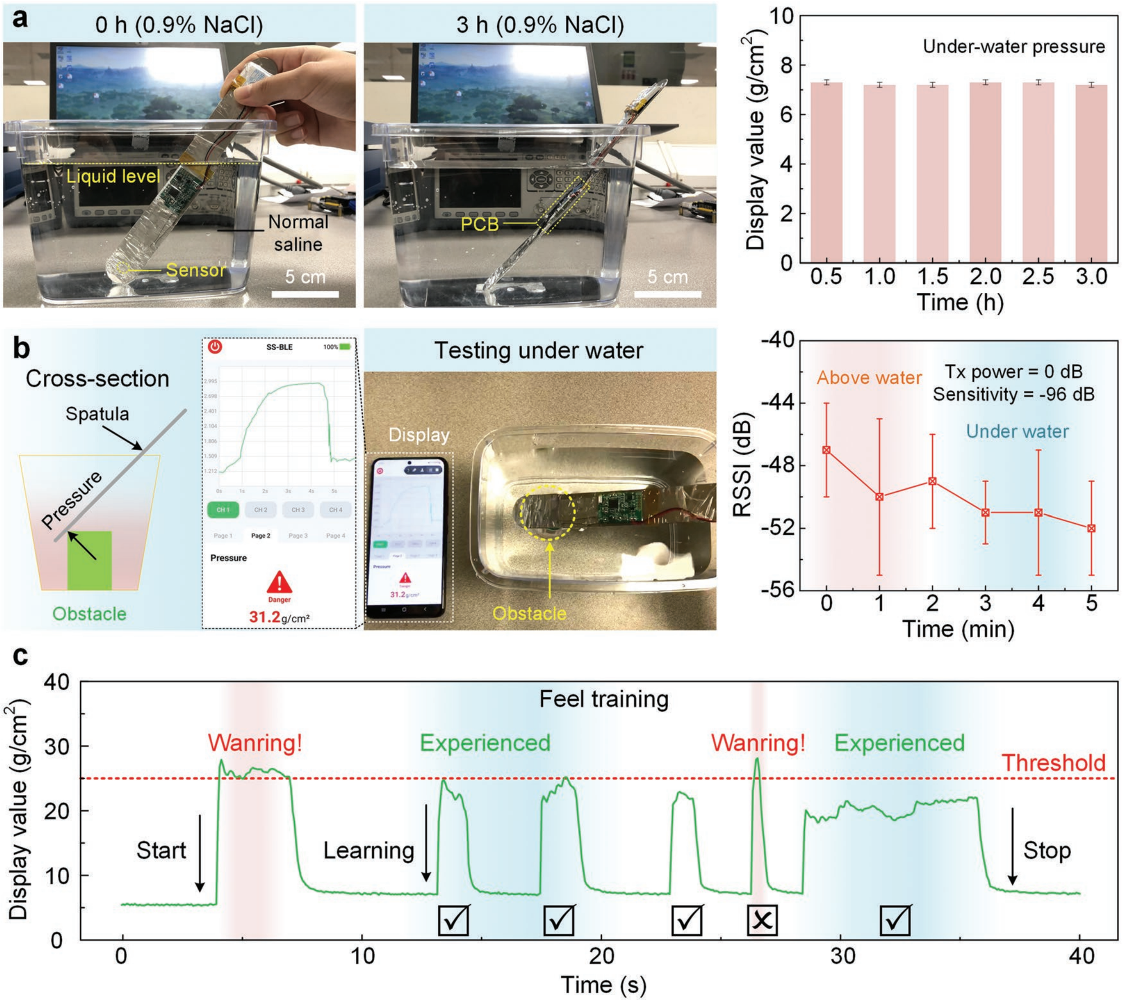

Figure 4. Sensing performance of underwater environments and relative applications. a) The static pressure response of spatula devices resting in normal saline. b) Real-time pressure monitoring of spatula devices under water with stable wireless communication stability. c) The feel training for controlling pressure under threshold using spatula devices.

several touching pressures are all within safe ranges (check mark) followed by another warning (cross mark). That is a normal training process, and thereby a faster learning route can be established using our spatula devices.

To confirm the stability of our device under other liquid besides normal saline, we also tested the long-time sensing performance under water mixed with artificial blood (**Figure 5**a). The artificial blood density (1.05 g cm^{-3}) is slightly larger than water (1.00 g cm^{-3}), and the displayed pressure value would have a shifting baseline along with increasing blood percentage. The detected pressure under pure artificial blood remained constant at approximately 7.3 g cm^{-2} after >3 h. The long-term stability of the sensing system in normal saline and artificial blood are also provided in Figure S7 (Supporting Information). Figure 5b demonstrates the applied pressure on a soft medical brain model (1:1 size) with brain spatula during repeated traction process. To gain an optimal inside view of brain tissue, the brain parenchyma is retracted multi times and the volunteer after several trainings can even handle this manipulation with few alarming. We also observed an interesting phenomenon: the displayed pressure is not only related to the immersion depth of spatula sensors but also closely correlated with the moving directions (see Video S2, Supporting Information). Figure 5c illustrates the sensing pressure versus time when the spatula is immersed under water. Each state would remain for several seconds to avoid much water disturbance. The pressure value is linearly correlated with the distance from the spatula sensor to the liquid level induced by liquid pressure ($p = \rho gh$, where ρ, g, and h stand for the liquid density, the gravitational acceleration and the aforementioned distance, respectively). This is why static pressures are always more than zero in Figure 4a. Note that the transient contact between spatula and water does not generate a drop-off value, which is inevitable for capacitive pressure sensors.[36] The changes in environmental permittivity, including blood, might cause considerable fluctuations in capacitive values, and the brain surgery requires more than subtle pressure detection. Therefore resistive pressure sensor would be more suitable to such situations. Besides, such sensors can also be potential for water-flow monitoring with reasonable designing pairs, with detailed analysis shown in Figure S8 (Supporting Information).

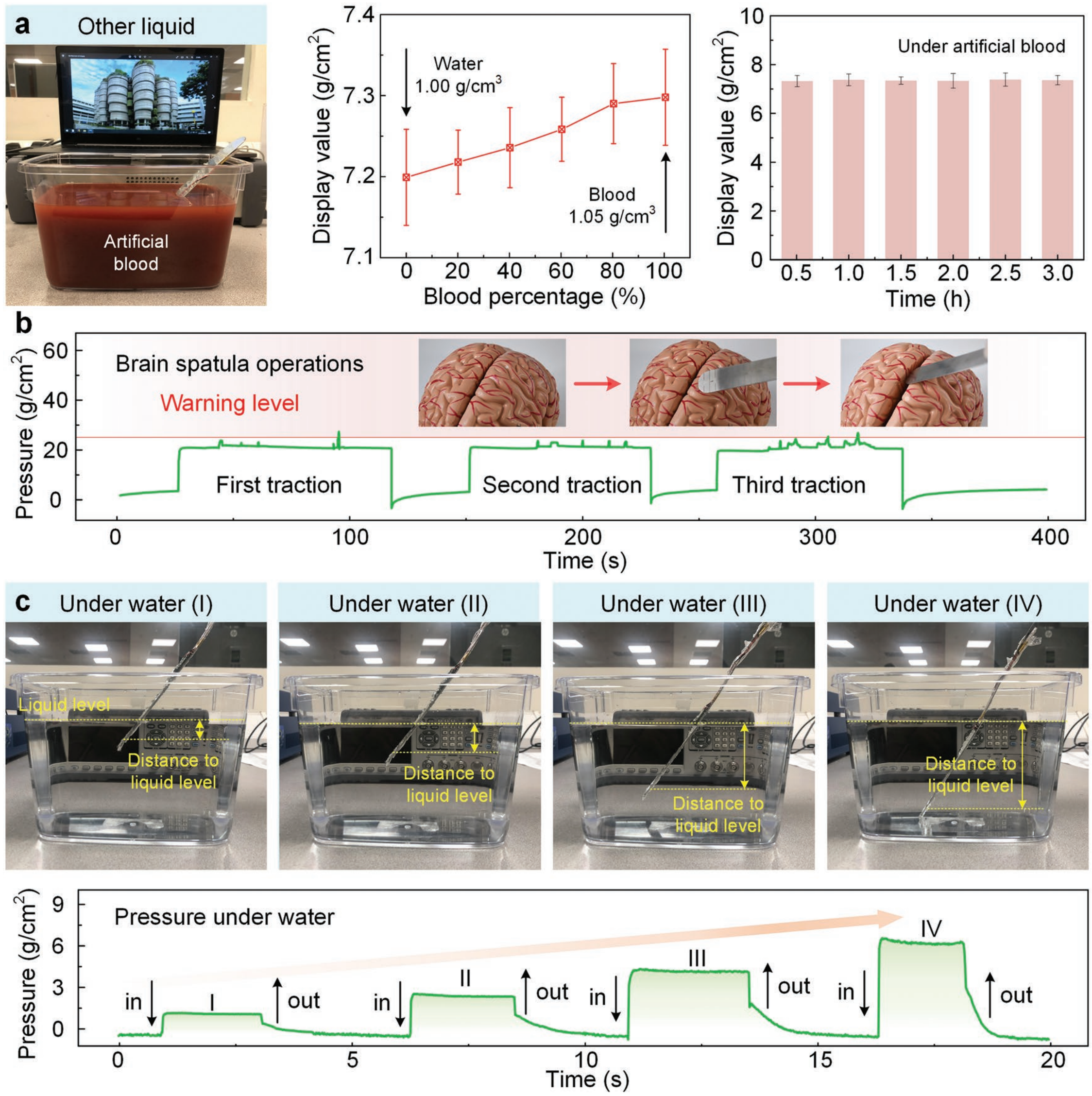

Figure 5. a) The long-time sensing performance under water mixed with artificial blood.b) The applied pressure on a soft medical brain model (1:1 size) with brain spatula during repeated traction process.c) Moving along different directions under water to sense water flow.

3. Conclusion

In this study, we have developed a wireless sensing system upon brain spatula, encapsulated by soft biocompatible materials. The system consists of stable resistive pressure sensors, tiny reading circuits with low power transmission functions and software-based model deployment. The ion gel-based construction of the micro-structured sensor represents key defining features, resulting in high measurement accuracy of 1.0/N with reliable water-proof capabilities. With our devices, detailed pressure data on retracting operations can be collected, analyzed, and stored for medical assistance as well as to improve surgery quality. The devices can also be used for feel training to realize the transition from inexperienced to experienced, as well as potential water flow monitoring. Overall, this work offers broad capabilities relevant to applications ranging from medical assistance to other pressure detection situations.

4. Experimental Section

Preparation of Ion Gel Films: First, 2 g of polyvinyl alcohol (PVA, Mw 145,000, from Aladdin Industrial Corporation) was dissolved into 18 g of deionized water, followed by stirring at 90 °C for 2 h until it dissolved completely. After the PVA solution cooled to room temperature (22 °C), 2 mL H_3PO_4 (AR, ≥ 85%, Shanghai Macklin Biochemical Co., Ltd.) was added and stirred for 2 h. The PVA/H_3PO_4 solution was then poured onto the PET film and cured at room temperature for 12 h. More details about the performance of different kinds of ion gel are given in Figure S9 (Supporting Information).

Fabrication of Sensors: The initial polyimide film (13 µm thick, on Polyethylene terephthalate supporting layer) was fixed onto the chamber substrate holder followed by consequent metal plating (Cu and Ni). An extra thin Au layer was followed to provide oxidation resistance and better weldability. PVA and H_3PO_4 solutions were mixed and cast on a flat glass substrate to be cured, followed by demolding. The microstructures were achieved on the cured resistive layer with ultra-high processing resolution, femtosecond laser to selectively remove surface materials. The femtosecond laser beam (with a pulse duration of 50 fs, central wavelength of 800 nm and repetition frequency of 1 kHz) from a Ti: sapphire laser system (Coherent, Librausp 1K-he200) was vertically focused onto the surface of the ion gel sheet by a plano-convex lens (focal length of 200 mm) in air. The ion gel substrate was fixed on a computer-controlled moveable platform. The laser power was held constant at 200 mW, and the moving speed of the platform was 3 mm s^{-1}. The laser-structured ion gel film can be seen in the Figure S10 (Supporting Information).

Fabrication of Electronics: The LDO was fabricated in SMIC 180 nm CMOS process, which occupies a chip area of 0.046 mm^2, with the die microphotograph. In this study, the LDO can support an input voltage range of 0.8–3.3 V and an output voltage range of 0.6–3.2 V. The maximum load current of the LDO is 201 mA with an external Capacitance of 1 µF for testing purposes and no internal capacitor was implemented on-chip. The average parameters of amplifier DC gain, unity-gain bandwidth, phase margin, and slew rate are 94.18 dB, 4.81 MHz, 58.42° and 2.53 V μs^{-1}, respectively. Besides, the error amplifier consumes little quiescent current and the maximum current efficiency of the LDO is 99.99%. Other commercial chips were also assembled on a sheet of fPCB into compact layouts. Solder paste (Chip Quik TS391LT) and a heat gun (AOYUE Int866) joined the various electronics and sensors onto the fPCB.

Silicone Protection and Assembling: The elastomeric protection sheet was formed by casting a silicone thermoset polymer into the gap formed by matching pairs of molds (Ecoflex, 00-30, smooth-on) with a thin thickness (0.3 mm). Curing occurred in an oven at 70 °C for 15 min. This design provided a waterproof encapsulation structure that also allowed free movement of the buckled serpentine lines. The gel was cured at room temperature in <30 min. The assembling and bonding were realized after silicone curing and assisted by an adhesive (loctite tak pak 444). The device showed no degradation in performance after complete immersion in phosphate buffered saline solution at 70 °C for 10 days.

Simulation and Characterizations of the Devices: Simulation of the pressing process was carried out using solid mechanics and electrical current modules in COMSOL Multiphysics 5.4. The sensors were set with one end constraint. The pressure force was simulated by a small displacement. The micro structure of encapsulating layer was observed by a FESEM (GeminiSEM 500, ZEISS). The resistance was also measured by a TongHui H2832 Precision LCR meter.

Statistical Analysis and Software Design: The participants were all recruited by the School of Electrical and Electronic Engineering Nanyang Technological University and entirely voluntary. For all the studies, the participant gave informed consent. The devices used were considered to carry minimal risk, and therefore approval was not needed. Collected data analysis was performed on MATLAB (R2018b) with technical computing language and Origin (2019b), and the initial quantitative analysis results of sensing parameters were obtained from 5 samples. The sensing model was converted into a lightweight version and deployed into Android on Android Studio (2021.1.1.23) with PyTorch Android lite library. The displayed mobile clients included a Samsung S22 (equipped with Android 12 system).

Supporting Information

Supporting Information is available from the Wiley Online Library or from the author.

Acknowledgements

Y.W., C.Z., and X.M. contributed equally to this work. This work was supported by the National Natural Science Foundation of China (No. 42074155 and No. 41574131), the PetroChina Innovation Foundation (No. 2019D-5007-0302), the Fundamental Research Funds for the Central Universities of China and the China Scholarship Council (No. 202006400062).

Conflict of Interest

The authors declare no conflict of interest.

Data Availability Statement

The data that support the findings of this study are available from the corresponding author upon reasonable request.

Keywords

brain spatula, flexible and compact electronics, real-time force detections, wirelessly communicating functions

Received: September 12, 2022
Revised: November 22, 2022
Published online: December 22, 2022

[1] M. Dujovny, O. Ibe, A. Perlin, T. Ryder, *Neurol. Res.* **2010**, *32*, 675.
[2] J. P. Greenfield, W. S. Cobb, A. J. Tsouris, T. H. Schwartz, *Neurosurg.* **2008**, *63*, 334.
[3] C. S. Hong, D. M. Prevedello, J. B. Elder, *J. Neurosurg.* **2016**, *124*, 799.
[4] G. B. Kaplan, J. J. Vasterling, P. C. Vedak, *Behav. Pharmacol.* **2010**, *21*, 427.
[5] M. Schneider, H. Schneider, A. Yassouridis, B. Saller, F. Von Rosen, G. Stalla, *Clin. Endocrinol.* **2008**, *68*, 206.
[6] A. Chodobski, B. J. Zink, J. Szmydynger-Chodobska, *Transl. Stroke Res.* **2011**, *2*, 492.
[7] M. F. Stiefel, J. D. Udoetuk, A. M. Spiotta, V. H. Gracias, A. Goldberg, E. Maloney-Wilensky, S. Bloom, P. D. Le Roux, *J. Neurosurg.* **2006**, *105*, 568.
[8] Y.-h. Bao, Y.-m. Liang, G.-y. Gao, Y.-h. Pan, Q.-z. Luo, J.-y. Jiang, *J. Neurotrauma* **2010**, *27*, 341.
[9] M. F. Stiefel, A. Spiotta, V. H. Gracias, A. M. Garuffe, O. Guillamondegui, E. Maloney-Wilensky, S. Bloom, M. S. Grady, P. D. LeRoux, *J. Neurosurg.* **2005**, *103*, 805.
[10] R. S. Karmakar, J.-C. Wang, Y.-T. Huang, K.-J. Lin, K.-C. Wei, Y.-H. Hsu, Y.-C. Huang, Y.-J. Lu, *ACS Omega* **2020**, *5*, 29342.
[11] M. Albin, L. Bunegin, M. Bennett, M. Dujovny, P. Jannetta, *Acta Neurol. Scand., Suppl.* **1977**, *64*, 522.
[12] A. Yokoh, K. Sugita, S. Kobayashi, *Acta Neurochir.* **1987**, *87*, 134.
[13] Y.-C. Huang, Y. Liu, C. Ma, H.-C. Cheng, Q. He, H. Wu, C. Wang, C.-Y. Lin, Y. Huang, X. Duan, *Nat. Electron.* **2020**, *3*, 59.
[14] S. C. Mannsfeld, B. C. Tee, R. M. Stoltenberg, C. V. Chen, S. Barman, B. V. Muir, A. N. Sokolov, C. Reese, Z. Bao, *Nat. Mater.* **2010**, *9*, 859.
[15] N. Bai, L. Wang, Q. Wang, J. Deng, Y. Wang, P. Lu, J. Huang, G. Li, Y. Zhang, J. Yang, K. Xie, X. Zhao, C. F. Guo, *Nat. Commun.* **2020**, *11*, 209.
[16] Z. Li, S. Zhang, Y. Chen, H. Ling, L. Zhao, G. Luo, X. Wang, M. C. Hartel, H. Liu, Y. Xue, R. Haghniaz, K. J. Lee, W. Sun, H. J. Kim, J. Lee, Y. Zhao, Y. Zhao, S. Emaminejad, S. Ahadian, N. Ashammakhi, M. R. Dokmeci, Z. Jiang, A. Khademhosseini, *Adv. Funct. Mater.* **2020**, *30*, 2003601.
[17] D. Kwon, T.-I. Lee, J. Shim, S. Ryu, M. S. Kim, S. Kim, T.-S. Kim, I. Park, *ACS Appl. Mater. Interfaces* **2016**, *8*, 16922.
[18] R. Yin, D. Wang, S. Zhao, Z. Lou, G. Shen, *Adv. Funct. Mater.* **2021**, *31*, 2008936.
[19] S. Chen, S. Xin, L. Yang, Y. Guo, W. Zhang, K. Sun, *Nano Energy* **2021**, *87*, 106178.

[20] S. Xiang, J. Tang, L. Yang, Y. Guo, Z. Zhao, W. Zhang, *npj Flexible Electron.* **2022**, *6*, 59.
[21] K. Lee, X. Ni, J. Y. Lee, H. Arafa, D. J. Pe, S. Xu, R. Avila, M. Irie, J. H. Lee, R. L. Easterlin, D. H. Kim, H. Uk Chung, O. O. Olabisi, S. Getaneh, E. Chung, M. Hill, J. Bell, H. Jang, C. Liu, J. B. Park, J. Kim, S. B. Kim, S. Mehta, M. Pharr, A. Tzavelis, J. T. Reeder, I. Huang, Y. Deng, Z. Xie, C. R. Davies, et al., *Nat. Biomed. Eng.* **2020**, *4*, 148.
[22] Y. Yang, Y. Song, X. Bo, J. Min, O. S. Pak, L. Zhu, M. Wang, J. Tu, A. Kogan, H. Zhang, T. K. Hsiai, Z. Li, W. Gao, *Nat. Biotechnol.* **2020**, *38*, 217.
[23] J. Kim, J. Park, Y.-G. Park, E. Cha, M. Ku, H. S. An, K.-P. Lee, M.-I. Huh, J. Kim, T.-S. Kim, D. W. Kim, H. K. Kim, J.-U. Park, *Nat. Biomed. Eng.* **2021**, *5*, 772.
[24] D.-H. Kim, J. Song, W. M. Choi, H.-S. Kim, R.-H. Kim, Z. Liu, Y. Y. Huang, K.-C. Hwang, Y.-w. Zhang, J. A. Rogers, *Proc. Natl. Acad. Sci. U. S. A.* **2008**, *105*, 18675.
[25] Z. Cui, W. Wang, L. Guo, Z. Liu, P. Cai, Y. Cui, T. Wang, C. Wang, M. Zhu, Y. Zhou, W. Liu, Y. Zheng, G. Deng, C. Xu, X. Chen, *Adv. Mater.* **2022**, *34*, 2104078.
[26] X. Liu, T.-C. Tang, E. Tham, H. Yuk, S. Lin, T. K. Lu, X. Zhao, *Proc. Natl. Acad. Sci. U. S. A.* **2017**, *114*, 2200.
[27] C. Wang, X. Chen, L. Wang, M. Makihata, H.-C. Liu, T. Zhou, X. Zhao, *Science* **2022**, *377*, 517.
[28] N. Bai, L. Wang, Y. Xue, Y. Wang, X. Hou, G. Li, Y. Zhang, M. Cai, L. Zhao, F. Guan, X. Wei, C. F. Guo, *ACS Nano* **2022**, *16*, 4338.
[29] V. Amoli, J. S. Kim, S. Y. Kim, J. Koo, Y. S. Chung, H. Choi, D. H. Kim, *Adv. Funct. Mater.* **2020**, *30*, 1904532.
[30] S. Chen, Y. Wang, L. Yang, Y. Guo, M. Wang, K. Sun, *Nano Energy* **2021**, *82*, 105719.
[31] X. Shuai, P. Zhu, W. Zeng, Y. Hu, X. Liang, Y. Zhang, R. Sun, C.-p. Wong, *ACS Appl. Mater. Interfaces* **2017**, *9*, 26314.
[32] S. Baek, H. Jang, S. Y. Kim, H. Jeong, S. Han, Y. Jang, D. H. Kim, H. S. Lee, *RSC Adv.* **2017**, *7*, 39420.
[33] C. Zhang, Z. Li, H. Li, Q. Yang, H. Wang, C. Shan, J. Zhang, X. Hou, F. Chen, *ACS Appl. Mater. Interfaces* **2022**, *14*, 38328.
[34] X. Liao, Q. Liao, X. Yan, Q. Liang, H. Si, M. Li, H. Wu, S. Cao, Y. Zhang, *Adv. Funct. Mater.* **2015**, *25*, 2395.
[35] S. Chen, G. Qian, B. Ghanem, Y. Wang, Z. Shu, X. Zhao, L. Yang, X. Liao, Y. Zheng, *Adv. Sci.* **2022**, *9*, 2203460.
[36] S. Chen, Y. Wang, L. Yang, F. Karouta, K. Sun, *Nano-Micro Lett.* **2020**, *12*, 136.